SPA: Shape-Prior Variational Autoencoders for Unsupervised Brain Pathology Segmentation

Cosmin I. Bercea[2,3] COSMIN.BERCEA@HELMHOLTZ-MUENCHEN.DE
Benedikt Wiestler[4] BENEDIKT.WIESTLER@TUM.DE
Daniel Rueckert[3,4,5] DANIEL.RUECKERT@TUM.DE
Shadi Albarqouni[1,2,3*] SHADI.ALBARQOUNI@UKBONN.DE
[1] *Clinic for Diagnostic and Interventional Radiology, University Hospital Bonn, Germany*
[2] *Helmholtz AI, Helmholtz Zentrum Muenchen, Neuherberg, Germany*
[3] *Technical University of Munich, Munich, Germany*
[4] *Klinikum Rechts der Isar, Munich, Germany*
[5] *Imperial College London, United Kingdom*

Editors: Under Review for MIDL 2022

Abstract

Deep unsupervised representation learning for brain pathology segmentation is of great interest for medical imaging, as it does not require extensive annotations for training and allows the detection of unseen pathologies. While recent approaches proposed to model the distribution of healthy brain Magnetic Resonance Imaging (MRI) using variational autoencoders, we propose to model the pixel distribution of the healthy brain by introducing a shape-prior based on the brain tissue distribution. To this end, we propose Shape-Prior variational Autoencoders (SPA) to disentangle the generative factors of brain MRI, namely cerebrospinal fluid (CSF), gray matter (GM), and white matter (WM). Our method obtains interpretable latent representations, providing pixel-wise tissue probability maps. We evaluated the proposed method on MRIs of 538 patients from six data-sets containing demyelinating lesions, small vessel disease, and tumors. Experimental results indicate that our method is capable of disentangling the generative brain MR factors and avoiding the reconstruction of anomalous regions, leading to better lesion detection performance.

Keywords: shape-prior, variational autoencoders, disentanglement, generative factors, brain anomaly detection

1. Introduction

The use of artificial intelligence for rapid and automated segmentation of abnormal structures is an important part of radiological assessment, improving clinical workflow and reducing the burden on radiologists (Hosny et al., 2018). Recently, many machine learning algorithms for identifying and segmenting critical MR findings of the brain have been proposed. Although supervised methods have been successfully applied to biomedical imaging (Ronneberger et al., 2015) and specifically to brain pathology segmentation (Baur et al., 2021b; Kamnitsas et al., 2016; Myronenko, 2019; Isensee et al., 2019; McKinley et al., 2019),

[*] Corresponding Author

their performance is limited by the amount and variety of annotated training data, which are sparse and expensive to collect. Furthermore, their performance in detecting abnormalities is constrained to the lesions present in the training dataset (Kamnitsas et al., 2017). To alleviate these issues, unsupervised lesion detection methods have been proposed. The underlying idea is that brain pathology can be identified as a deviation of the healthy brain distribution. As an early attempt, (Leemput et al., 2001) utilized registration to a healthy brain atlas and modeled the pixel intensities using tissue-specific probabilistic priors to detect lesions. Based on a similar concept, (Moon et al., 2002) used an atlas prior with spatial features, and (Marcel et al., 2004) combined spatial and intensity based atlas priors. (Aït-Ali et al., 2005; Freifeld et al., 2007) use probabilistic Gaussian Mixture Models (GMM) to detect and segment multiple sclerosis (MS) lesions. More recently, convolutional autoencoders are able to extract more powerful representations and are used to compress and encode healthy brain scans, then learn how to reconstruct the data back as close to the original input as possible. This allows localization and segmentation of pathology from faulty reconstructions of abnormal samples (Schlegl et al., 2017; Chen and Konukoglu, 2018; Pawlowski et al., 2018; Baur et al., 2021a; Bercea et al., 2021a; Silva-Rodrguez et al., 2021). However, autoencoders are prone to over-fitting (Steck, 2020). Variational autoencoders (VAEs) (Kingma and Welling, 2014) overcome this issue by approximating the distribution of high dimensional data and were successfully applied to brain anomaly detection (Zimmerer et al., 2018, 2019; Pinaya et al., 2021). Gaussian mixture variational autoencoders allow more complex representation in the latent space and extend VAEs to replace the uni-model Gaussian prior with a mixture of Gaussians (Dilokthanakul et al., 2017). The closest to our proposed method is the work by (You et al., 2019), who applied GMVAEs to unsupervised brain anomaly detection. In this work, we introduce novel Shape-Prior variational Autoencoders (SPA) for unsupervised brain pathology segmentation, see Figure 1. While the GMMs capture the variation in the healthy brain manifold, we propose to combine the traditional efforts in modeling the pixel distributions with the representation power and generalization capability of VAEs. To realize this, we build a probabilistic shape prior to enforce the latent disentanglement of the brain MR generative factors, namely cerebrospinal fluid (CSF), gray matter (GM), and white matter (WM). At inference, our method obtains interpretable latent representations, providing pixel-wise tissue probability maps. These probabilistic maps are then decoded to pseudo-healthy reconstructions of pathological samples, which when subtracted from the original input, results in the localization and segmentation of anomalous regions. We validate the proposed method on MR scans of 538 patients from six data-sets containing demyelinating lesions, small vessel disease, and tumors and show superior performance. Additionally, we provide insight into the latent tissue disentanglement of healthy and pathological data.

2. Methods

2.1. SPA: Shape-Prior variational Autoencoders

In contrast to previous works, we combine traditional modeling of pixel distributions with tissue-specific probabilistic brain priors with the representation power of modern VAEs. We formulate the latent variable model as $\log p(X) = \log \int p(X|Z)p(Z)dZ$, with $X \in \mathbb{R}^{H \times W}$ the image, $Z \in \mathbb{R}^{H \times W \times K}$ the latent variable and $p(Z)$ the tissue-specific probabilistic prior.

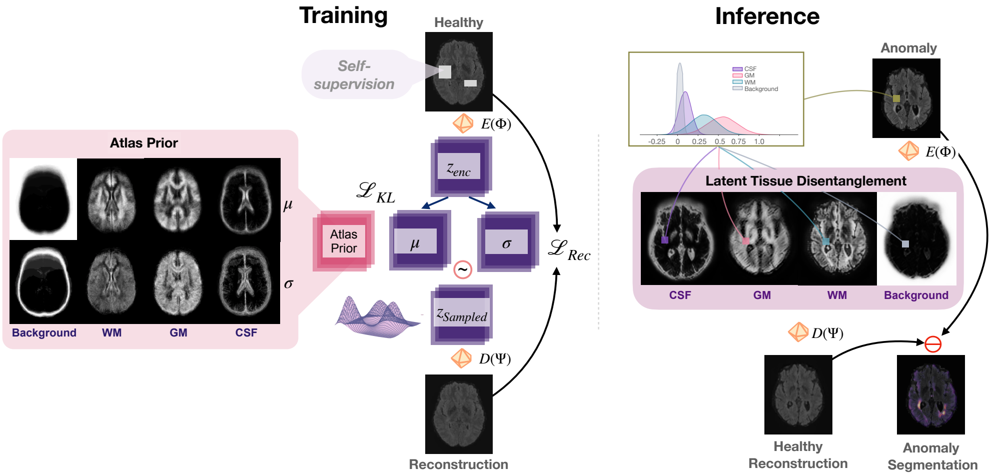

Figure 1: The proposed novel Shape-Prior variational Autoencoder disentangles the pixel-wise latent generative factors of brain MR, namely cerebrospinal fluid (CSF), gray matter (GM), and white matter (WM). The anomaly segmentation is given by the residual of the input image and its pseudo-healthy reconstruction.

To this end, we introduce the shape-prior $p(Z)$ based on the tissue distribution of healthy patients. We model every pixel i in $p(Z)$ as a Gaussian-mixture model given by:

$$p(Z_i) = \sum_{c=1}^{K} \pi_{c,i} \cdot \mathcal{N}(\mu_{c,i}, \sigma_{c,i}) \tag{1}$$

with K being the number of components of the mixture model: here we use $K = 4$ clusters to explicitly model the tissue channels given by CSF, GM, WM, and background; and $\mathcal{N}(\mu_{c,i}, \sigma_{c,i})$ represents the distribution of the probability of pixel i belonging to cluster c of a healthy population. Our objective is to maximize the log-likelihood, $\log p(X)$ of the observed samples. As the integral is intractable, we approximate the true posterior $p(Z|X)$ with a proposal distribution $q(Z|X)$ as introduced in (Kingma and Welling, 2014).

$$\log p(X) \geq ELBO = \mathbb{E}_{q(Z|X)}[\log p(X|Z)] - KL[q(Z|X)||p(Z)], \tag{2}$$

where KL denotes the Kullback-Leibler divergence; the encoder $q(Z|X)$, projects the input X to the latent space Z and is parameterized by the neural network $E(\Phi)$; the decoder $p(X|Z)$, reconstructs the $\hat{X}$ from Z and it is parameterized by the neural network $D(\Psi)$.

2.2. Disentangled Representations

Disentangled learning of the latent representation are achieved by weighting the KL divergence loss term in Equation 2 with a β term (Higgins et al., 2017). Thus, our objective is to optimize the following loss term:

$$\arg\min_{\Phi\Psi} \sum_{X} \mathcal{L}_{Rec}(X, \hat{X}) + \beta \mathcal{L}_{KL}(E(X; \Phi), p(Z)), \tag{3}$$

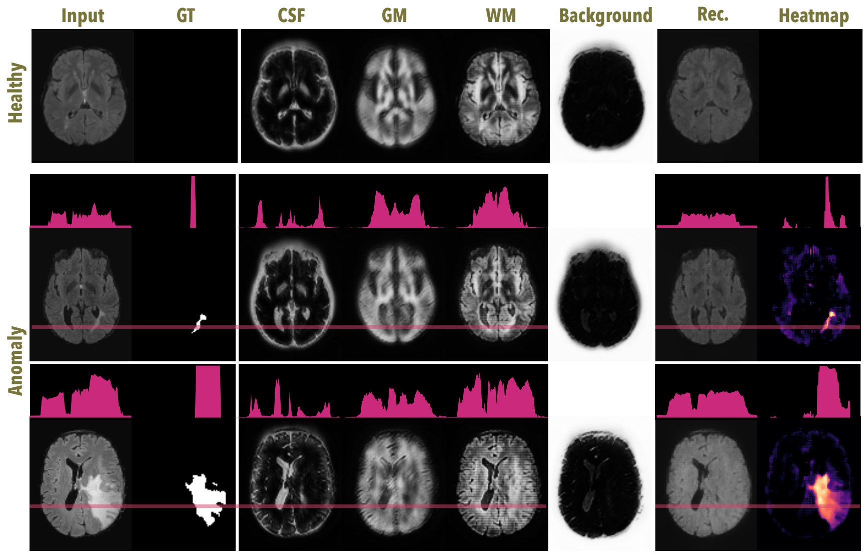

Tissue	DICE↑
CSF	0.346 ± 0.032
GM	0.456 ± 0.031
WM	0.49 ± 0.018
Bckg	0.97 ± 0.004

Figure 2: Visualization of the latent tissue disentanglement. The first row shows the results on healthy data, and the next two rows show tissue probability maps in presence of anomalies. Line integrals (magenta) visualize the intensity of the pixels along the line.

where $\mathcal{L}_{Rec} = \frac{1}{H \times W} \sum_{i=0}^{H \times W} |X - \hat{X}| + TV(\hat{X}) + \lambda PL(X, \hat{X})$, β is used to weight the influence of the prior, and $\mathcal{L}_{KL}$ is the KL divergence. To enforce high-resolution and smooth reconstructions, we follow prior work for style transfer and super-resolution (Johnson et al., 2016) and add a perceptual loss and total variation regularizer to the usual mean absolute error. The main benefit of using the additional loss terms is the increased reconstruction accuracy, i.e., SSIM on healthy test data of 0.954 compared to 0.807 in our previous work (Bercea et al., 2021b). We use the same loss function for all the baselines to ensure a fair comparison. Finding the right β term in practice is tedious. Due to the strong influence of the prior distribution, the resulting latent representations are often oversimplified and do not adequately reflect the underlying structure of the data (Dilokthanakul et al., 2017). As we show in section 4 this problem also occurs in our method and degenerates the latent tissue disentanglement. Current solutions require exhaustive search either for an annealing parameter to slowly incorporate the KL term during training (Sønderby et al., 2016), or for a cutoff threshold to stop optimizing the KL term (Kingma et al., 2017). Inspired by the signal processing literature, we propose a heuristic based on a given signal-to-noise ratio (SNR) to achieve both good reconstruction fidelity and latent regularization. Specifically, we adapt the reparameterization trick from $\mu + \sigma \odot \eta$ to:

$$\mu + \frac{1}{\sqrt{SNR}} \cdot \frac{||\mu||}{||\eta||} \cdot \sigma \odot \eta$$

where $\odot$ is the Hadamard product, $|| \cdot ||$ is the ℓ_2-norm, and $\eta \sim \mathcal{N}(0, I)$.

Table 1: Datasets details

	HI	MSLUB	MSISBI	MSI	WMH	GBI	BRATS
Train/Val/Test	125/15/23	-/-/30	-/-/21	-/-/48	-/-/60	-/-/94	-/-/285
Cohort	Healthy	Multiple Sclerosis			Vascular lesions	Brain tumors	
Age	69 ± 4	39 ± 10	N/A	32 ± 10	N/A	61 ± 20	60 ± 9
Sex (% female)	56	76	N/A	61	N/A	50	N/A
Scanner (3T)	Philips Achieva	Siemens Intera	Philips Achieva	Philips Achieva	Philips& Siemens &GE Diverse	Siemens Verio	Multiple (N=19)
Res (mm)	$1.5 \times 0.9 \times 0.9$	$0.8 \times 0.47 \times 0.47$	$2.2 \times 0.82 \times 0.82$	$1.5 \times 0.9 \times 0.9$	Diverse	$1.5 \times 0.9 \times 0.9$	$1 \times 1 \times 1$
TR/TE/TI (s)	10/0.14/2.75	5/0.392/1.8	11/0.068/2.8	10/0.14/2.75	Diverse	5/0.395/1.8	Diverse

All images were re-sampled to $1 \times 1 \times 1$ mm, skull-stripped, and registered to the SRI-24 atlas (Rohlfing et al., 2010)

3. Experimental setup

Datasets, Implementation and Hyperparameters. Details of the used datasets are shown in section 3. The healthy (HI), MS lesions (MSI) and glioblastoma (GBI) internal databases are provided by Klinikum Rechts der Isar in Munich. We use public datasets of MSLUB (Lesjak et al., 2018), MSISBI (Carass et al., 2017), WMH(Kuijf et al., 2019), and BraTS (Menze et al., 2015; Bakas et al., 2017, 2019). Both the common encoder $E(\Phi)$ and decoder $D(\Psi)$ follow the original U-Net description by Ronneberger et al. (Ronneberger et al., 2015), but adjusted the network to handle input at a 128 × 128 resolution. The resulting network has 3 blocks each for encoding and decoding. The composition of a block is as follows: $2 \times [3 \times 3$ convolutions with filters $\in \{32, 64, 128\}$, batch normalization and LeakyReLu activation]. The mean and log sigma estimation of VAEs is implemented using two convolution only layers with a kernel size of 1. For the implementation of SPA, we additionally add a *sigmoid* and *logsigmoid* activation layers to bring the estimated distribution in the range of the prior. We follow (You et al., 2019) for the GMVAE latent implementation. We derived the distribution of the tissue specific probabilistic prior on 136 healthy patients from our healthy internal dataset HI. We calculated the mean and variance of the atlas distribution by averaging segmentation maps of CSF, GM, WM and background of 136 healthy patients, that were obtained using the antsAtroposN4.sh script (Avants et al., 2009). Note that, our method is not dependent on the derived atlas and can be extended with any distribution over the tissue-specific probability maps. For all baselines, we used self-supervision techniques as described in (Bercea et al., 2021b) to enforce healthy reconstructions and trained the networks until convergence with a batch size of 2, and ADAM optimizer with a learning rate of $5 \cdot 10^{-4}$ and exponential decay of 0.97. We set the $\lambda := 0.1, \beta := 10^{-3}$, and $SNR := 16$ as discussed in section 4.

Pre- and post-processing. Similar to (Baur et al., 2021a), all scans have been registered to the SRI24 atlas template space (Rohlfing et al., 2010) and have subsequently been skull-stripped with ROBEX (Iglesias et al., 2011) and normalized to the [0,1] range. We used all axial slices with visible tissue information with a size of 128×128px for training and evaluation. We keep the absolute residual of the input and its reconstruction. We use the generated heat maps to compute AUPRC and binarize the results using a threshold τ to compute the maximum DICE scores per dataset.

Evaluation metrics. We observe both L1 and KL losses on validation data for the model selection. To measure the anomaly segmentation performance and compare different models,

Table 2: We show AUPRC to assess anomaly detection on six datasets with pathology. We compare our method to sota unsupervised models without any post-processing (Baur et al., 2021a), namely: context VAE (c-VAE) (Zimmerer et al., 2018), constrained adversarial AEs (cAAE) (Chen and Konukoglu, 2018), f-AnoGAN (Schlegl et al., 2017), and Gaussian-mixture VAEs with image restoration (GM-IR) (You et al., 2019); two variational baselines with the same training and implementation details as our network; and two supervised methods based on U-Net (Ronneberger et al., 2015). (*) shows results with simple post-processing (keeping positive residual and applying median filtering of size 3); and ($^\bullet$) shows results on a validation subset; **bold**/$\underline{\text{underscore}}$ show the best two results among baselines.

Training	Sota Unsupervised - AUPRC ↑								AUPRC ↑		
	Healthy								Supervised		Thresh.
Method	c-VAE	cAAE	f-AnoGAN	GM-IR	VAE	GMVAE	SPA	SPA*	MSLUB	BraTS	n/a
MSLUB	0.030	0.035	0.034	0.037	$\underline{0.059}$	**0.078**	$\underline{0.059}$	0.132	0.420$^\bullet$	0.049	0.150
MSISBI	0.023	$\underline{0.027}$	**0.035**	0.025	0.007	0.011	0.023	0.019	0.423	0.020	0.135
MSI	0.027	0.036	0.041	0.036	0.092	$\underline{0.162}$	**0.178**	0.389	0.478	0.094	0.114
WMH	n/a				0.027	$\underline{0.101}$	**0.159**	0.167	0.407	0.147	0.280
GBI	0.052	0.076	0.061	0.086	0.160	$\underline{0.209}$	**0.234**	0.453	0.267	0.463	0.367
BraTS	n/a				0.104	$\underline{0.215}$	**0.320**	0.397	0.350	0.751$^\bullet$	0.473

we report the area under the precision $TP/(TP+FP)$ - recall $TP/(TP+FN)$ curves (AUPRC), with TP, FP, and FN being true positives, false positives and false negatives.

4. Results

We experimentally validated our method on multiple institutes with real pathological datasets containing MS-, vascular-, and brain tumor lesions. Our main findings are i) we successfully disentangle the generative factors of brain MR imaging, namely, the CSF, GM, WM, and background; ii) we avoid the reconstruction of unwanted pathological features; and consequently iii) we improve the anomaly detection performance.

Latent Tissue Disentanglement. Our proposed method aims at disentangling the generative factors of brain MR and provide latent pixel-wise tissue probability maps. Figure 2 provide quantitative and qualitative results of the learned latent representations. We show the Dice score of predicted tissue maps on 30 healthy unseen test subjects. Visually, the tissue segmentation maps capture the underlying anatomy and intracranial tissue distribution despite the lower Dice scores. In particular for CSF one can observe a tendency to also segment CSF surrounding the brain, where the skull would normally be. However, considering that a small rim of (sub)dural CSF surrounds the brain and the space surrounding it has a very similar (low) intensity as CSF on these FLAIR images as a result of the skull stripping, the segmentation makes sense. The first row in the figure visualizes the tissue probability maps on a healthy patient, followed by two examples containing pathology. The provided intensity profiles show the intensity of the pixels along the marked line. Note that, while anomalies correspond to a peak in the intensity profile of the input, finding a common threshold for both cases is not straightforward. For example, the peak in the first row would correspond to the intensity of healthy tissue of the second case. Interestingly,

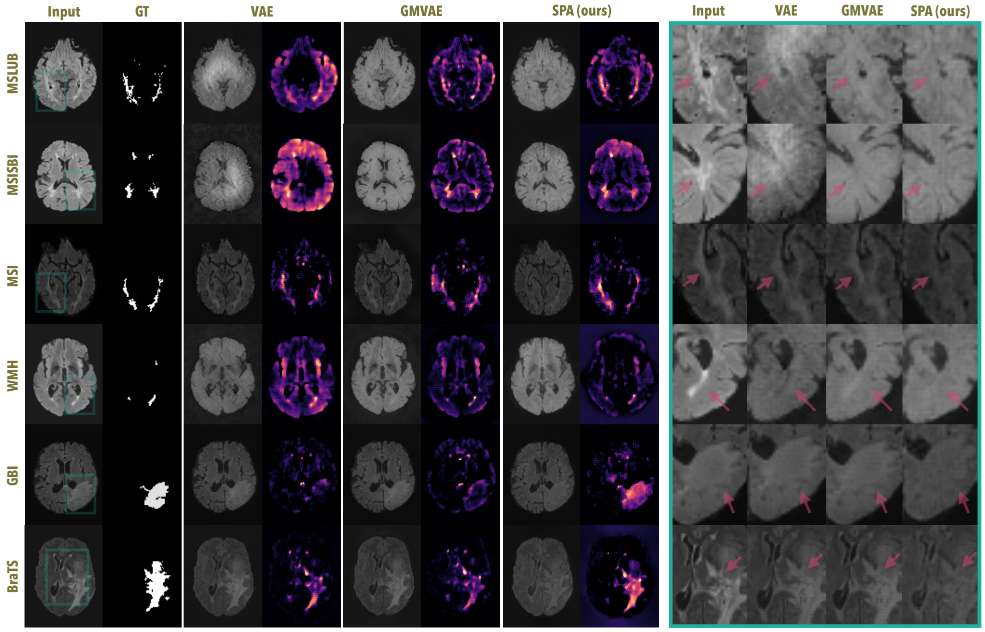

Figure 3: Qualitative results of our method compared to the VAE and GMVAE baselines. The first columns show the input and ground truth segmentation mask followed by reconstructions and residual heatmaps for the different datasets (rows). The last four columns show a zoomed-in image highlighting the reconstruction of unwanted pathological features.

the anomalous regions are either encoded as WM or GM in the latent tissue maps, having the same probability as healthy tissues. The decoder will thus only reconstruct intensities of healthy tissues containing CSF, GM, and WM, as can be seen in the line profiles. Finally, note that due to the pseudo-healthy reconstructions, the residual maps and their line profiles are very similar to the ground truth, making anomalies easy to detect.

Anomaly Segmentation. Table 2 shows the anomaly segmentation performance of our proposed method. We outperform sota unsupervised anomaly detection methods without any post-processing, see Table 8 in (Baur et al., 2021a) and achieve an average improvement (AUPRC) of $154.5\%, 177.5\%$ and 35.5% over the best unsupervised method, GM-IR, and variational baselines VAE and GMVAE, respectively. Compared to supervised methods, our proposed method outperforms or achieves competitive anomaly results with different U-Net variants. Even though not directly comparable, a supervised U-Net validated on the dataset it was trained on achieves the best results. This indicates that our method generalizes better to unseen domains, and that the performance of supervised method is degraded on pathologies not seen during training, reconfirming the results in (Baur et al., 2021b). The commonly used approach in clinical practice is a naive threshold-based classifier that selects hyper-intense regions. With just a simple post-processing step (keeping positive residuals and applying a median filter of size 3) our method achieves remarkable relative DICE improvement on MSLUB (24%), MSI (293%), and GBI (16%) and slightly worse on MSISBI, WMH and BraTS, reconfirming the findings of (Baur et al., 2021a) that tumors might be quite challenging since it might contain lesions that do not appear as hyperintensity

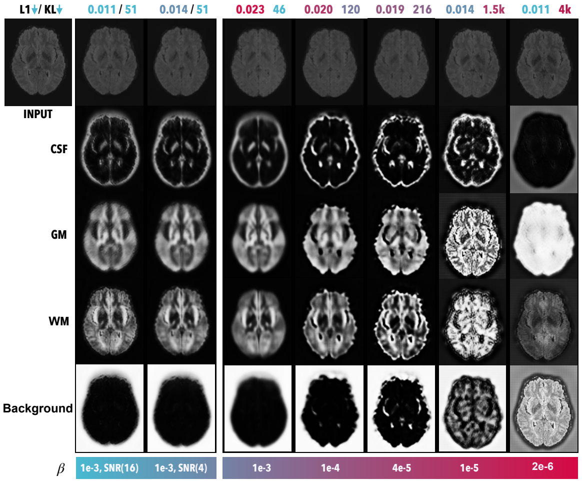

Method →	Baselines				Ours	
	AE		GMVAE		PMVAE	
$\beta \downarrow$	L1	KL	L1	KL	L1	KL
$1e^{-3}$, S16	0.009	1	0.007	1	0.011	51
$1e^{-3}$, S4	0.015	1	0.009	1	0.014	51
$1e^{-3}$	0.023	16	0.028	13	0.023	46
$1e^{-4}$	0.020	120	0.023	126	0.020	120
$4e^{-5}$	0.018	320	0.020	350	0.019	216
$1e^{-5}$	0.012	2k	0.013	2k	0.014	1.5k
$2e^{-6}$	0.008	7k	0.010	7k	0.011	4k

Figure 4: Model Selection. We show quantitative and qualitative results on the healthy validation set for multiple choices of β. We set β to $1e^{-3}$ and SNR to 16 for our experiments.

in FLAIR, and naive thresholding should be still considered as a strong baseline(Meissen et al., 2021). Figure 3 gives more insight into the network's predictions. Our method avoids the reconstruction of pathology (best seen in the last columns) and delivers more accurate segmentation masks.

Sensitivity to β values. Figure 4 shows quantitative and qualitative results of the effect of β. Note that, high values of β enforce the posterior to match the prior atlas distribution, however at the cost of the reconstruction accuracy. Setting β to lower values yields better reconstructions, but the posterior diverges from the prior atlas distribution. Finding the balance between the two is a tedious task and leads in most cases to either a compromise on the reconstruction or regularization. The β values of 10^{-3} and SNR of 16 achieve the best validation results in terms of reconstruction loss and KL divergence for all methods.

5. Discussion and future work

In this paper, we proposed Shape-Prior variational AEs (SPA), to combine traditional modeling of pixel distribution of brain MR based on tissue probabilistic priors and the representation and generalizability of VAEs. We generate the probabilistic shape prior once, offline, from affine-registered healthy scans to avoid the requirement of good alignment of input scans during inference. We have showed that our method provides interpretable pixel-level latent tissue segmentation maps, enforces the anomalous pixels to be mapped to the healthy pixel-wise distribution and considerably improves the results without post-processing over sota unsupervised methods. However, post-processing steps are still critical for better results and their effects should be studied in the future. We find that our method performs best on datasets that follow the same distribution as the healthy training set and plan to investigate and address the domain shift in data from multiple institutes and its impact on generalization with the help of disentanglement and federated learning.

References

L. S. Aït-Ali, S. Prima, P. Hellier, B. Carsin, G. Edan, and C. Barillot. Strem: A robust multidimensional parametric method to segment ms lesions in mri. In James S. Duncan and Guido Gerig, editors, *Medical Image Computing and Computer-Assisted Intervention – MICCAI 2005*, pages 409–416, Berlin, Heidelberg, 2005. Springer Berlin Heidelberg. ISBN 978-3-540-32094-4.

Brian B Avants, Nick Tustison, Gang Song, et al. Advanced normalization tools (ants). *Insight j*, 2(365):1–35, 2009.

S Bakas, H Akbari, A Sotiras, M Bilello, M Rozycki, JS Kirby, JB Freymann, K Farahani, and Davatzikos C. Advancing the cancer genome atlas glioma mri collections with expert segmentation labels and radiomic features. *Sci Data*, 2017.

Spyridon Bakas, Mauricio Reyes, Andras Jakab, Stefan Bauer, Markus Rempfler, Weiwei Zong, Jayashree Kalpathy-Cramer, Keyvan Farahani, Christos Davatzikos, Koen van Leemput, and Bjoern Menze. Identifying the best machine learning algorithms for brain tumor segmentation, progression assessment, and overall survival prediction in the brats challenge, 2019.

Christoph Baur, Stefan Denner, Benedikt Wiestler, Nassir Navab, and Shadi Albarqouni. Autoencoders for unsupervised anomaly segmentation in brain mr images: A comparative study. *Medical Image Analysis*, page 101952, 2021a.

Christoph Baur, Benedikt Wiestler, Mark Muehlau, Claus Zimmer, Nassir Navab, and Shadi Albarqouni. Modeling healthy anatomy with artificial intelligence for unsupervised anomaly detection in brain mri. *Radiology: Artificial Intelligence*, 3(3):e190169, 2021b.

Cosmin I. Bercea, Benedikt Wiestler, Daniel Rueckert, and Shadi Albarqouni. Feddis: Disentangled federated learning for unsupervised brain pathology segmentation, 2021a.

Cosmin I. Bercea, Benedikt Wiestler, Daniel Rueckert, and Shadi Albarqouni. Federated disentangled representation learning for unsupervised brain anomaly detection. *PREPRINT (Version 1) available at Research Square*, 2021b.

Aaron Carass, Snehashis Roy, Amod Jog, Jennifer L. Cuzzocreo, Elizabeth Magrath, Adrian Gherman, Julia Button, James Nguyen, Pierre-Louis Bazin, Peter A. Calabresi, Ciprian M. Crainiceanu, Lotta M. Ellingsen, Daniel S. Reich, Jerry L. Prince, and Dzung L. Pham. Longitudinal multiple sclerosis lesion segmentation data resource. *Data in Brief*, 12:346–350, 2017. ISSN 2352-3409.

Xiaoran Chen and Ender Konukoglu. Unsupervised detection of lesions in brain mri using constrained adversarial auto-encoders. *arXiv preprint arXiv:1806.04972*, 2018.

Nat Dilokthanakul, Pedro A. M. Mediano, Marta Garnelo, Matthew C. H. Lee, Hugh Salimbeni, Kai Arulkumaran, and Murray Shanahan. Deep unsupervised clustering with gaussian mixture variational autoencoders, 2017.

Oren Freifeld, Hayit Greenspan, and Jacob Goldberger. Lesion detection in noisy mr brain images using constrained gmm and active contours. In *2007 4th IEEE International Symposium on Biomedical Imaging: From Nano to Macro*, pages 596–599, 2007. doi: 10.1109/ISBI.2007.356922.

Irina Higgins, Loïc Matthey, Arka Pal, Christopher Burgess, Xavier Glorot, Matthew Botvinick, Shakir Mohamed, and Alexander Lerchner. beta-vae: Learning basic visual concepts with a constrained variational framework. In *5th International Conference on Learning Representations, ICLR 2017, Toulon, France, April 24-26, 2017, Conference Track Proceedings*. OpenReview.net, 2017. URL https://openreview.net/forum?id=Sy2fzU9gl.

Ahmed Hosny, Chintan Parmar, John Quackenbush, Lawrence H Schwartz, and Hugo JWL Aerts. Artificial intelligence in radiology. *Nature Reviews Cancer*, 18(8):500–510, 2018.

Juan Eugenio Iglesias, Cheng-Yi Liu, Paul M Thompson, and Zhuowen Tu. Robust brain extraction across datasets and comparison with publicly available methods. *IEEE transactions on medical imaging*, 30(9):1617–1634, 2011.

Fabian Isensee, Philipp Kickingereder, Wolfgang Wick, Martin Bendszus, and Klaus H. Maier-Hein. No new-net. In Alessandro Crimi, Spyridon Bakas, Hugo Kuijf, Farahani Keyvan, Mauricio Reyes, and Theo van Walsum, editors, *Brainlesion: Glioma, Multiple Sclerosis, Stroke and Traumatic Brain Injuries*, pages 234–244, Cham, 2019. Springer International Publishing. ISBN 978-3-030-11726-9.

Justin Johnson, Alexandre Alahi, and Li Fei-Fei. Perceptual losses for real-time style transfer and super-resolution, 2016.

Konstantinos Kamnitsas, Christian Ledig, Virginia F. J. Newcombe, Joanna P. Simpson, Andrew D. Kane, David K. Menon, Daniel Rueckert, and Ben Glocker. Efficient multiscale 3d CNN with fully connected CRF for accurate brain lesion segmentation. *CoRR*, abs/1603.05959, 2016. URL http://arxiv.org/abs/1603.05959.

Konstantinos Kamnitsas, Christian Baumgartner, Christian Ledig, Virginia Newcombe, Joanna Simpson, Andrew Kane, David Menon, Aditya Nori, Antonio Criminisi, Daniel Rueckert, and Ben Glocker. Unsupervised domain adaptation in brain lesion segmentation with adversarial networks. In Marc Niethammer, Martin Styner, Stephen Aylward, Hongtu Zhu, Ipek Oguz, Pew-Thian Yap, and Dinggang Shen, editors, *Information Processing in Medical Imaging*, pages 597–609, Cham, 2017. Springer International Publishing. ISBN 978-3-319-59050-9.

Diederik P Kingma and Max Welling. Auto-encoding variational bayes, 2014.

Diederik P. Kingma, Tim Salimans, Rafal Jozefowicz, Xi Chen, Ilya Sutskever, and Max Welling. Improving variational inference with inverse autoregressive flow, 2017.

Hugo J Kuijf, J Matthijs Biesbroek, Jeroen De Bresser, Rutger Heinen, Simon Andermatt, Mariana Bento, Matt Berseth, Mikhail Belyaev, M Jorge Cardoso, Adria Casamitjana, et al. Standardized assessment of automatic segmentation of white matter hyperintensities and results of the wmh segmentation challenge. *IEEE transactions on medical imaging*, 38(11):2556–2568, 2019.

Koen Van Leemput, Frederik Maes, Dirk Vandermeulen, Alan C. F. Colchester, and Paul Suetens. Automated segmentation of multiple sclerosis lesions by model outlier detection. *IEEE Trans. Medical Imaging*, 20(8):677–688, 2001.

Ziga Lesjak, Alfiia Galimzianova, Ales Koren, Matej Lukin, Franjo Pernus, Bostjan Likar, and Ziga Spiclin. A novel public mr image dataset of multiple sclerosis patients with lesion segmentations based on multi-rater consensus. *Neuroinformatics*, 16, 01 2018.

Prastawa Marcel, Bullitt Elizabeth, Ho Sean, and Gerig Guido. A brain tumor segmentation framework based on outlier detection. *Med Image Anal.*, 2004.

Richard McKinley, Raphael Meier, and Roland Wiest. Ensembles of densely-connected cnns with label-uncertainty for brain tumor segmentation. In Alessandro Crimi, Spyridon Bakas, Hugo Kuijf, Farahani Keyvan, Mauricio Reyes, and Theo van Walsum, editors, *Brainlesion: Glioma, Multiple Sclerosis, Stroke and Traumatic Brain Injuries*, pages 456–465, Cham, 2019. Springer International Publishing. ISBN 978-3-030-11726-9.

Felix Meissen, Georgios Kaissis, and Daniel Rueckert. Challenging current semi-supervised anomaly segmentation methods for brain mri. *arXiv preprint arXiv:2109.06023*, 2021.

BH Menze, A Jakab, S Bauer, J Kalpathy-Cramer, K Farahani, J Kirby, Y Burren, N Porz, J Slotboom, R Wiest, and Weber MA Arbel T Avants BB Ayache N Buendia P Collins DL Cordier N Corso JJ Criminisi A Das T Delingette H Demiralp Durst CR Dojat M Doyle S Festa J Forbes F Geremia E Glocker B Golland P Guo X Hamamci A Iftekharuddin KM Jena R John NM Konukoglu E Lashkari D Mariz JA Meier R Pereira S Precup D Price SJ Raviv TR Reza SM Ryan M Sarikaya D Schwartz L Shin HC Shotton J Silva CA Sousa N Subbanna NK Szekely G Taylor TJ Thomas OM Tustison NJ Unal G Vasseur F Wintermark M Ye DH Zhao L Zhao B Zikic D Prastawa M Reyes M Van Leemput K. Lanczi L, Gerstner E. The multimodal brain tumor image segmentation benchmark (brats). *IEEE Trans Med Imaging*, 2015.

Nathan Moon, Elizabeth Bullitt, Koen Van Leemput, and Guido Gerig. Automatic brain and tumor segmentation. In *Medical Image Computing and Computer-Assisted Intervention MICCAI 2002. Volume 2489 of LNCS*, pages 372–379. Springer Verlag, 2002.

Andriy Myronenko. 3d mri brain tumor segmentation using autoencoder regularization. In Alessandro Crimi, Spyridon Bakas, Hugo Kuijf, Farahani Keyvan, Mauricio Reyes, and Theo van Walsum, editors, *Brainlesion: Glioma, Multiple Sclerosis, Stroke and Traumatic Brain Injuries*, pages 311–320, Cham, 2019. Springer International Publishing. ISBN 978-3-030-11726-9.

Nick Pawlowski, Matthew CH Lee, Martin Rajchl, Steven McDonagh, Enzo Ferrante, Konstantinos Kamnitsas, Sam Cooke, Susan Stevenson, Aneesh Khetani, Tom Newman, et al. Unsupervised lesion detection in brain ct using bayesian convolutional autoencoders. 2018.

Walter Hugo Lopez Pinaya, Petru-Daniel Tudosiu, Robert Gray, Geraint Rees, Parashkev Nachev, Sebastien Ourselin, and M. Jorge Cardoso. Unsupervised brain anomaly detection and segmentation with transformers, 2021.

Torsten Rohlfing, Natalie M Zahr, Edith V Sullivan, and Adolf Pfefferbaum. The sri24 multichannel atlas of normal adult human brain structure. *Human brain mapping*, 31(5): 798–819, 2010.

Olaf Ronneberger, Philipp Fischer, and Thomas Brox. U-net: Convolutional networks for biomedical image segmentation. In Nassir Navab, Joachim Hornegger, William M. Wells, and Alejandro F. Frangi, editors, *Medical Image Computing and Computer-Assisted Intervention – MICCAI 2015*, pages 234–241, Cham, 2015. Springer International Publishing.

Thomas Schlegl, Philipp Seebck, Sebastian M. Waldstein, Ursula Schmidt-Erfurth, and Georg Langs. Unsupervised anomaly detection with generative adversarial networks to guide marker discovery, 2017.

Julio Silva-Rodrguez, Valery Naranjo, and Jose Dolz. Looking at the whole picture: constrained unsupervised anomaly segmentation, 2021.

Casper Kaae Sønderby, Tapani Raiko, Lars Maaløe, Søren Kaae Sønderby, and Ole Winther. How to train deep variational autoencoders and probabilistic ladder networks. *arXiv preprint arXiv:1602.02282*, 3, 2016.

Harald Steck. Autoencoders that don't overfit towards the identity. *Advances in Neural Information Processing Systems*, 33:19598–19608, 2020.

Suhang You, Kerem Tezcan, Xiaoran Chen, and Ender Konukoglu. Unsupervised lesion detection via image restoration with a normative prior. In *International Conference on Medical Imaging with Deep Learning*, London, United Kingdom, 08–10 Jul 2019. URL https://openreview.net/forum?id=S1xg4W-leV.

David Zimmerer, Simon A. A. Kohl, Jens Petersen, Fabian Isensee, and Klaus H. Maier-Hein. Context-encoding variational autoencoder for unsupervised anomaly detection, 2018.

David Zimmerer, Fabian Isensee, Jens Petersen, Simon Kohl, and Klaus Maier-Hein. Unsupervised anomaly localization using variational auto-encoders, 2019.

Appendix A. Quantitative Metrics

Table 3 shows area under precision-recall curve for supervised U-Net (Ronneberger et al., 2015) trained and evaluated on different datasets. Table 4 shows the best achievable DICE and mean hausdorff distance (HD). Table 5 shows results with a simple post-processing step, where we keep the positive residual, instead of the absolute error since pathology tends to appear as hyper-intense regions in FLAIR sequences and apply median filtering of size 3 to the result.

Table 3: We show AUPRC to assess the anomaly detection performance on six different datasets with pathology for supervised methods based on U-Net (Ronneberger et al., 2015)

Method →	AUPRC ↑					
Trained on	Supervised					
Task ↓	U-Net(Ronneberger et al., 2015)					
	MSLUB	MSISBI	MSKRI	WMH	GBKRI	BraTS
MSLUB	0.420$^{\bullet}$	0.423	**0.478**	0.407	0.267	0.350
MSISBI	0.262	0.536$^{\bullet}$	0.162	**0.480**	0.136	0.156
MSI	0.328	0.158	0.656$^{\bullet}$	**0.466**	0.174	0.176
WMH	0.234	**0.501**	0.135	0.516$^{\bullet}$	0.145	0.191
GBI	0.102	0.015	0.264	0.060	0.551$^{\bullet}$	**0.454**
BraTS	0.049	0.020	0.094	0.147	**0.463**	0.751$^{\bullet}$

Table 4: We show the maximum DICE scores per dataset given by $2TP/(2TP+FP+FN)$ and the mean hausdorff distance $\lceil HD \rceil$ to assess the anomaly detection performance on six datasets with pathology.

Dataset	$\lceil Dice \rceil$ ↑				$\lceil HD \rceil$ ↓			
	VAE	GMVAE	SPA(Ours)	Thresh.	VAE	GMVAE	SPA (Ours)	Thresh.
MSLUB	0.133	**0.185**	0.136	0.219	**30.2**	32.1	31.2	24.0
MSISBI	0.022	0.029	**0.055**	0.208	49.9	49.4	**37.6**	24.1
MSI	0.210	**0.306**	0.275	0.157	**29.4**	32.3	35.3	23.7
WMH	0.073	0.204	**0.241**	0.327	34.6	33.0	36.3	25.3
GBI	0.260	0.281	**0.313**	0.386	39.1	**38.4**	44.3	24.3
BraTS	0.209	0.297	**0.388**	0.443	37.7	**35.3**	57.3	21.6

Table 5: Results with simple post-processing (keeping just positive residuals and applying median filtering of size 3). We show AUPRC, the maximum DICE scores per dataset given by $2TP/(2TP+FP+FN)$ and the mean hausdorff distance $\lceil HD \rceil$ to assess the anomaly detection performance on six datasets with pathology.

	AUPRC ↑			
Dataset	VAE	GMVAE	SPA(Ours)	Thresh.
MSLUB	0.051	0.128	**0.132**	0.135
MSISBI	0.006	0.015	**0.019**	0.119
MSI	0.162	0.312	**0.389**	0.091
WMH	0.087	0.098	**0.167**	0.278
GBI	0.165	0.384	**0.453**	0.432
BraTS	0.087	0.324	**0.397**	0.487

Dataset	$\lceil Dice \rceil \uparrow$				$\lceil HD \rceil \downarrow$			
	VAE	GMVAE	SPA (Ours)	Thresh.	VAE	GMVAE	SPA (Ours)	Thresh.
MSLUB	0.110	0.190	**0.217**	0.175	29.2	**26.1**	29.4	28.2
MSISBI	0.027	0.036	**0.044**	0.176	35.8	**31.4**	35.6	28.9
MSI	0.242	0.376	**0.437**	0.111	**24.7**	25.7	25.3	24.8
WMH	0.160	0.201	**0.224**	0.318	35.5	**33.2**	33.7	29.7
GBI	0.258	0.395	**0.496**	0.427	30.4	29.4	**29.2**	23.0
BraTS	0.185	0.415	**0.421**	0.446	54.0	28.6	**26.2**	20.6